University of Iceland

Computational electroreduction of CO_2 into sustainable fuel using copper nanoparticles

Author:
Kristinn Ingi Guðmundsson

Advisors:
Egill Skúlason
Javed Hussain

January 25, 2018

Abstract

Calculations were done for electrochemical CO_2 reduction to both methanol and methane formation on three copper nanoparticles that differ by size and configuration; 55 atom particle (Cu55) and two different 78 atom particles (Cu78-type1 and Cu78-type2) along with a Cu147 NP. The calculations predict the lowest free energy pathway along with their onset potentials, which is the applied potential needed to start the reactions. The calculations were done using density functional theory using both the BEEF-vdW and the RPBE density functionals. The onset potentials were compared with previous results from an extended Cu(111) surface. We predict Cu55, Cu78-type1, Cu78-type2 and Cu147 NPs to have onset potentials of 0.86 V, 0.78 V,0.82 V and 0.87 V respectively, which is very close to the onset potential of the Cu(111) surface of 0.81 V. Therefore, these results indicate that the CO_2 onset potential for the nanoparticles considered in this work do not differ much from the flat surface.

1 Introduction

The reduction of carbon dioxide into synthetic fuels is a very hot topic due to the increasing carbon emission to the atmosphere in the last few decades. These emissions have been found to be the leading cause of the greenhouse effect which is causing a global increase in temperature. This rise in temperature could lead to ecological catastrophe if messures are not put into place to halt these carbon emissions. Thus the incentive to find new methods of obtaining sustainable fuels is very high. One way to do this is the reduction of CO_2 electrochemically through $CO2$ electroreduction reaction (CER). The effectiveness of this process is highly reliant on the catalyst used in the reduction, as it must reduce CO_2 both efficiently and without unwanted biproducts. Finding a catalyst which can reduce CO_2 efficiently under ambient conditions would greatly advance the process towards producing carbon neutral fuel.

During his work, Hussain et al found two simple descriptors, which specify what main product is to be expected from a electrocatalyst. The goal of this study is to apply this simple model to bimetallic alloys, and perform a high throughput screening to investigate which bimetallic alloy candidates are worth performing more detailed studies on. Promising candidates will be submitted to more detailed study.

Density functional theory (DFT) can be used to get better insight into the characteristics of the reduction reaction of CO_2 using many different catalysts. Pure transition metals have already been analyzed and of all the pure metals, only copper has been found to work. Reducing the size of the nanoparticles (NPs) can also further increase efficiency of the catalyst due to increasing surface area on the NP. The icosahedral structure has been experementally proven to be the most stable NP and in this report we intend on analyze its properties.

2 Methodology

Electronic structure calculations were performed using density functional theory (DFT) with the Bayesian error estimation functional (BEE-vdW) and the revised Perdew-Burke-Ernzerhof Functionals (RPBE) exchange-correlation functional in a plane wave pseudopotential implementation using the VASP calculation package. The calculations were done on the (111) plane and edges of a Cu55 icosahedral NP, along the edge of the Cu78-type1 NP, on multiple sites on the Cu78-type2 NP, on the (111) plane and the edges of the Cu147 NP. The atomic structure of the various reactants and products was found by minimizing the energy until atomic forces had dropped below 0.03 ev / angstrom. The adsorbates that were investigated are those who can take part in the hydrogenation of CO_2. The final energy of the following adsorbant groups involved in the hydrogenation were calculated and used to determine the most likely route : CO_2, $COOH$, CO, COH, CHO, $CHOH$, CH_2O, CH_2OH, CH_3O, CH_3OH, CH, $CH2$, CH_3, H_2O, H,O, C and OH. The Cu55 particle was calculated straight via BEEF while both the Cu78 particles and the Cu147 NP were calculated

using RPBE, then calculated in BEEF using single point calculation, which have been found to be close to the method of direct BEEF calculation.

The lowest energy structures of the 3 NP were found by Anna Garden in New Zealand via the following method: A population of 20 copper clusters (either Cu55 or Cu78) was created. Each cluster was formed by randomly placing Cu atoms within a unit cell and locally minimizing it using the BFGS optimizer, where the energy of the cluster was described by the Gupta potential.

The population was subjected to the genetic algorithm. In the genetic algorithm, 16 offspring were created from the clusters in the population. These 16 offspring were created either by the weighed cut and splice method of mating or starting from scratch and randomly placing Cu atoms within a blank unit cell (as was done to initialize the population). The offspring were further locally minimized using the BFGS optimizer where the energy to minimize was described by the Gupta potential. A modified population was created from the 20 lowest energy clusters from the 20 clusters in the original population and the 16 off spring from the current generation. This is typically called "Natural Selection" in the genetic algorithm. This new population was called the first "generation".

This process of generating generations by creating offspring and performing natural selection on the population was repeated 625 times. The genetic algorithm ended when either 625 generations were performed or if all the clusters in the population were of the exact same energy to two decimal places.

The adsorbants sites were found for each of the NP via the following methods:

For the Cu55 NP, each of these adsorbants were placed onto initial sites on the NP. The sites were: the FCC hole site (I-hole)and the HCP hole site (O-hole) on the (111) plane, the middle atom of an edge (M-edge), the corner of and edge (C-edge) and the bridge between the corner and the middle on the edge (B-edge).

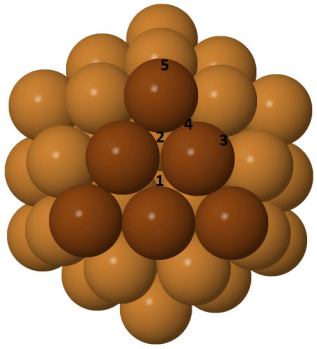

Figure 1: The figure shows the locations of the I-hole site (site 1), O-hole site (site 2), M-edge site (site 3), C-edge site (site 4) and the B-edge site (site 5) on a (111) facet (tinted darker).

The Cu78-type1 NP was has a Cu55 icosahedron as a base and then a outer Cu23 shell which is in the shape of a incomplete, next order, outermost layer of a icosahedral structure (Cu147). The assumption was made that the most likely bonding site would be on the edge between the growing 23 Cu layer and the

Cu55 section and 17 sites were checked along half the edge along with 2 sites on on the top and bottom of the particle for comparison.

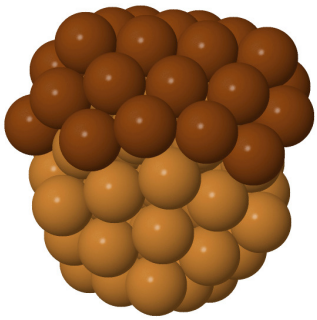

Figure 2: The figure shows the structure of Cu78-type1 NP with the growing Cu23 layer tinted darker

The Cu78-type2 NP contained two icosahedron-like "tops" half sandwiching an order array of Cu atoms about the belly of the structure. Due to the uncertainty of where the best adsorption sites were prompted us to check multiple sites on the NP. First the adsorption of CO was investigated and the sites narrowed down to 11, then further narrowed down to 4 after cheking the adsorbtion of CHO and COH. The rest of the adsorbates were then checked on those sites.

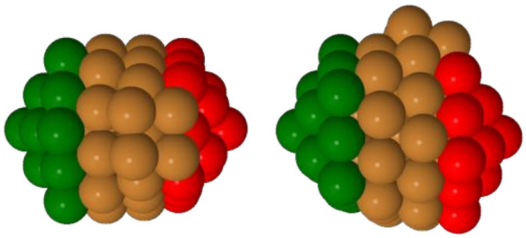

Figure 3: The figure shows the structure of Cu78-type2 NP with the left side being a view from the top and the right side being a view from the side and with the green and red ares being the "tops".

The Cu147 NP adsorbant included 10 unique adsorbtion sites. 2 HCP hole sites, 1 FCC hole sites, 2 bridge sites on the (111) surface, 2 bridge sites on the edge along with 3 sites on top of atoms (the atom in the middle of the (111) surface, the atom on the middle of the edge and the corner atom). For each adsorbant, only the sites on the Cu147 NP similar to thoes sites which were good at adsorbing the respective adsorbant on the Cu55 NP were checked in order to reduce the calculation time.

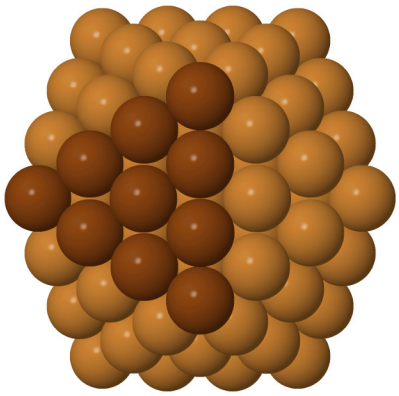

Figure 4: The figure shows the structure of the base Cu147 NP with one of its (111) surfaces tinted darker

A Cu (111) layer was used in this paper as a refrence and to compare the NP to an equivalent bulk surface.

The bond energy (ΔE_{DFT}) of a adsorbant group on a site was then acquired by subtracting the bare NP and the calculated energy of the atoms C,H and O in the adsorbant, which was calculated by simulating H2, H2O and graphene, from the final energy of the NP with the adsorbant. Then, from the bonding energy and using known constants of $\Delta ZPE, T\Delta S$ and $C_P\Delta T$, the Gibbs free energy (ΔG)was calculated for each adsorbant using the following equation:

$$\Delta G = \Delta E_{DFT} + \Delta ZPE - T\Delta S + C_P\Delta T \tag{1}$$

Then multiple pathways were analyzed and the best for each product chemical ere identified along with analysis from a comparison (111)-layer pathway.

The zero voltage in this theory is based on the reversible hydrogen electrode (RHE) . It can be interpreted with the following equation:

$$\mathrm{H^+ + e^-} \rightleftharpoons \frac{1}{2}\,\mathrm{H_2} \tag{2}$$

where at zero voltage the equation above is at equilibrium for all stages of PH, temperatures and at standard atmospheric pressure (101,325 kPa). However, in our model, the chemical potential of the proton-electron pair is half the electron potential of the gaseous hydrogen at the 0V potential and thus we can calculate the proton-electron potential can be calculated from the H_2 chemical potential. This chemical potential can be changed as a function of an applied potential using the following standard relation between chemical and electrical potential:

$$\Delta G = -neU \tag{3}$$

where e is the elementary positive charge , N is a whole number and U is the applied bias.

3 Results

3.1 Cu55 NP

3.1.1 Free energy Diagram

The calculations were carried out on the Cu55 NP. All the best adsorbent sites were found around the (111)-facets terrace of Cu55. The intermediates for the first two elementary steps in the LEP in electrochemical CO_2 reduction to methane, adsorbed very well. The third elementary step (*CO + ($H^+ + e^-$) –> *CHO), is the most endothermic step in the LEP and thus is the potential limiting step (PLS). The COH intermediate reported in the LEP for electrochemical CO2 reduction to methane reported by Hussain et al. on Cu(111) is about 0.6 eV more unstable than CHO, hence this species is not an intermediate for the pathway found here on Cu55. We also investigated different confirmation for each intermediate, and have specfied in green (*COH), blue (*CHOH) and red (*CH_2OH) in figure 5. The same pathway can be branched out to either methane or methanol, once we have *CH_3O species on the surface.

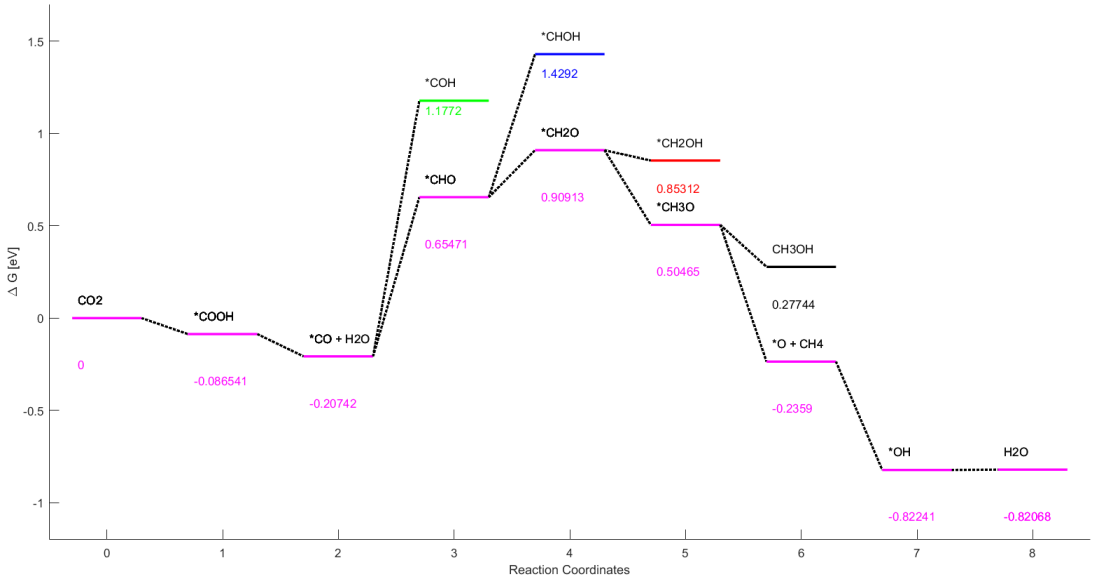

Figure 5: The figure shows FED of the Cu55 NP with both methane and methanol pathways alongside other pathways.

3.1.2 CH_4Production

Best pathway for CH_4 production on the Cu55 NP was identified as

$$CO_2 \rightarrow^* COOH \rightarrow^* CO \rightarrow^* CHO \rightarrow^* CH_2O \rightarrow^* CH_3O \rightarrow^* O \rightarrow^* OH \rightarrow H_2O \tag{4}$$

where * denotes that the chemical compound is adsorbed onto the NP.

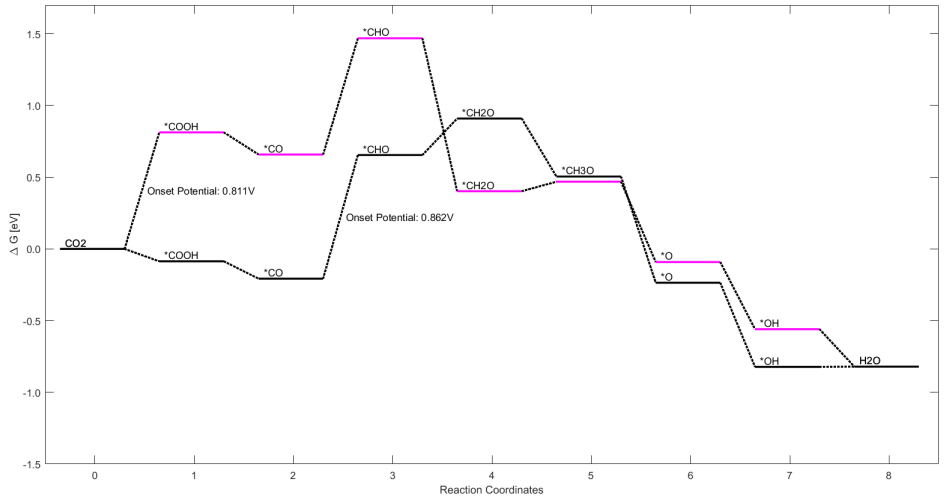

Figure 6: The figure shows the free energy diagram of the best CH_4 producing pathway on the Cu55 NP along with the same pathway on a (111) Cu layer

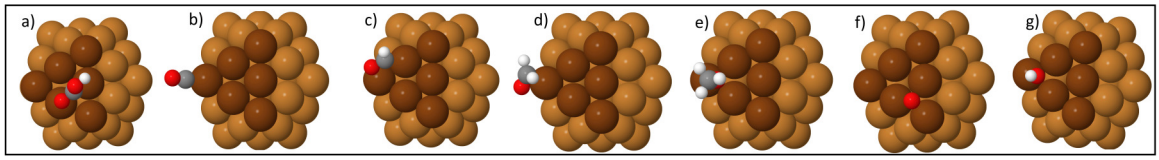

Figure 7: The figure shows the adsorbtion sites of the best pathway for CH_4 with the chemicals being: a)$COOH$, b)CO, c)CHO, d)CH_2O, e)CH_3O, f)O, g)OH

3.1.3 CH_3OH Production

Best pathway for CH_3OH production was identified as

$$CO_2 \rightarrow^* COOH \rightarrow^* CO \rightarrow^* CHO \rightarrow^* CH_2O \rightarrow^* CH_3O \rightarrow^* CH_3OH \tag{5}$$

where * denotes that the chemical compound is adsorbed onto the NP.

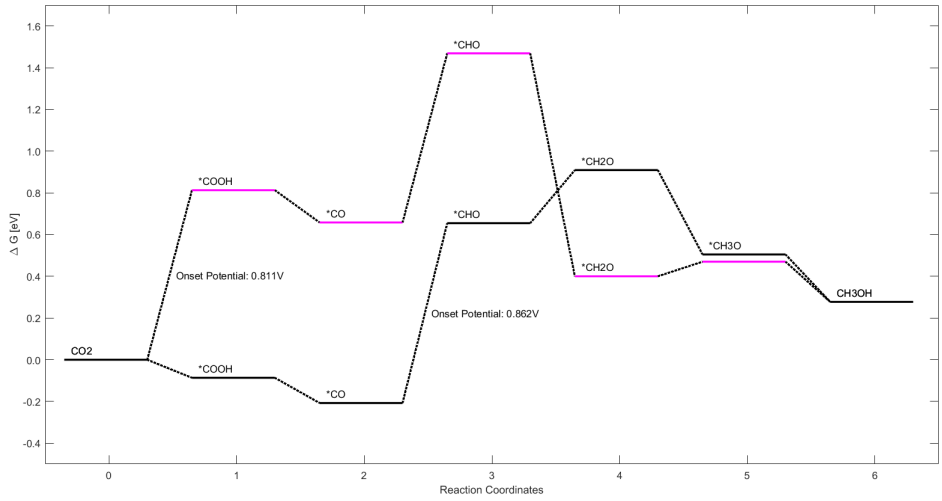

Figure 8: The figure shows the free energy diagram of the best CH_3OH producing pathway on the Cu55 NP along with the same pathway on a (111) Cu layer

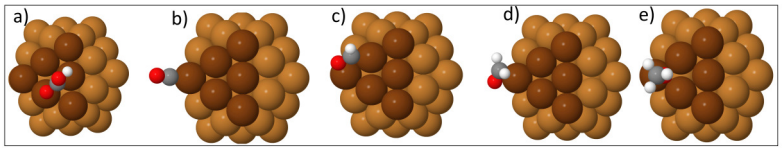

Figure 9: The figure shows the adsorbtion sites of the best pathway for CH_3OH production with the chemicals being: a)$COOH$, b)CO, c)CHO, d)CH_2O, e)CH_3O

Adsorbate	Optimized structure	E_b	Adsorbate	Optimized structure	E_b
$^*COOH$		1.101	$^*CO$	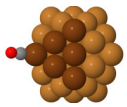	0.710
$^*CHO$		1.292	$^*COH$		2.005
$^*CHOH$		1.697	$^*CH_2O$		0.897
$^*CH_2OH$		0.811	$^*CH_3O$	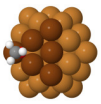	-0.078
$^*CH_3$		-0.049	$^*CH_2$		0.917
$^*H_2O$	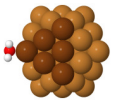	-0.319	$^*H$		-0.131
$^*O$		0.545	$^*OH$	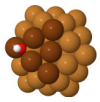	-0.112
$^*C$		2.478	$^*CH$		1.337

Table 1: Table of the adsorbate groups, their adsorbation sites and their bonding energy on a Cu55 NP.

3.2 Cu78-type1 NP

3.2.1 Free energy Diagram

The best adsorption sites were found along the edge on the side of the NP. The LEP in general has better absorption of intermediates than the Cu55 NP, resulting on *COOH and *CO + H_2O having lower energy than CO2, and *OH having lower energy than H_2O. The onset potential of the LEP is lower than the Cu55 NP. This pathway has the same PLS as the Cu55 NP.

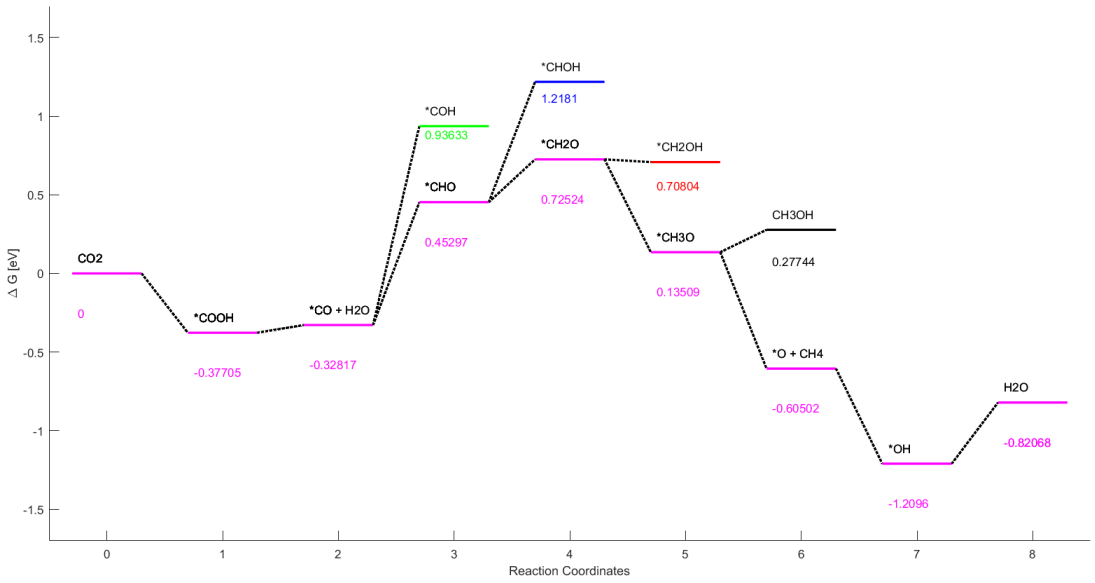

Figure 10: The figure shows FED of the Cu78-type1 NP with both methane and methanol pathways alongside other pathways.

3.2.2 CH_4 Production

Best pathway for CH_4 production on the Cu78-type1 NP was identified as

$$CO_2 \rightarrow^* COOH \rightarrow^* CO \rightarrow^* CHO \rightarrow^* CH_2O \rightarrow^* CH_3O \rightarrow^* O \rightarrow^* OH \rightarrow H_2O \tag{6}$$

where * denotes that the chemical compound is adsorbed onto the NP.

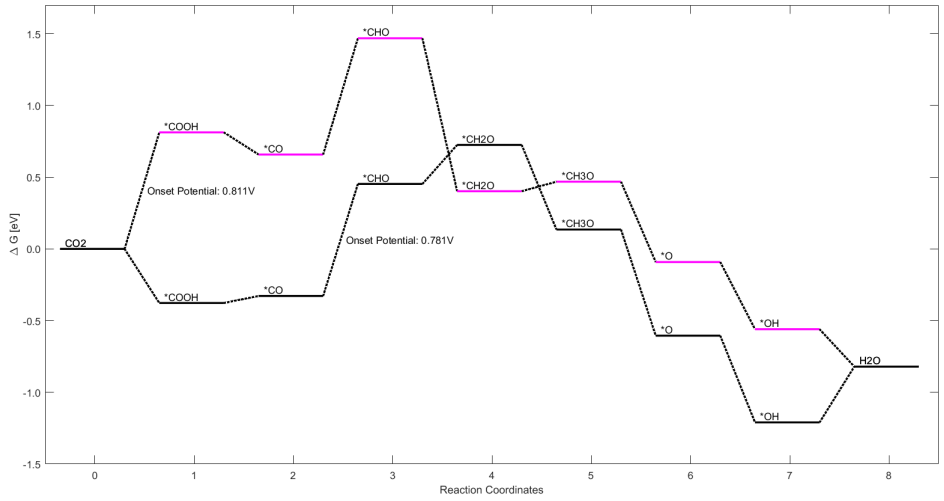

Figure 11: The figure shows the free energy diagram of the best CH_4 producing pathway on the Cu78-type1 NP along with the same pathway on a (111) Cu layer

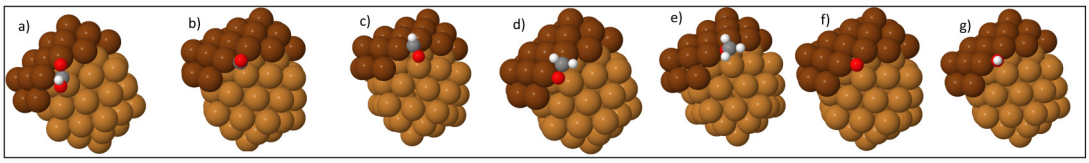

Figure 12: The figure shows the adsorbtion sites of the best pathway for CH_4 with the chemicals being: a)$COOH$, b)CO, c)CHO, d)CH_2O, e)CH_3O, f)O, g)OH

3.2.3 CH_3OH Production

Best pathway for CH_3OH production was identified as

$$CO_2 \rightarrow^* COOH \rightarrow^* CO \rightarrow^* CHO \rightarrow^* CH_2O \rightarrow^* CH_3O \rightarrow^* CH_3OH \tag{7}$$

where * denotes that the chemical compound is adsorbed onto the NP.

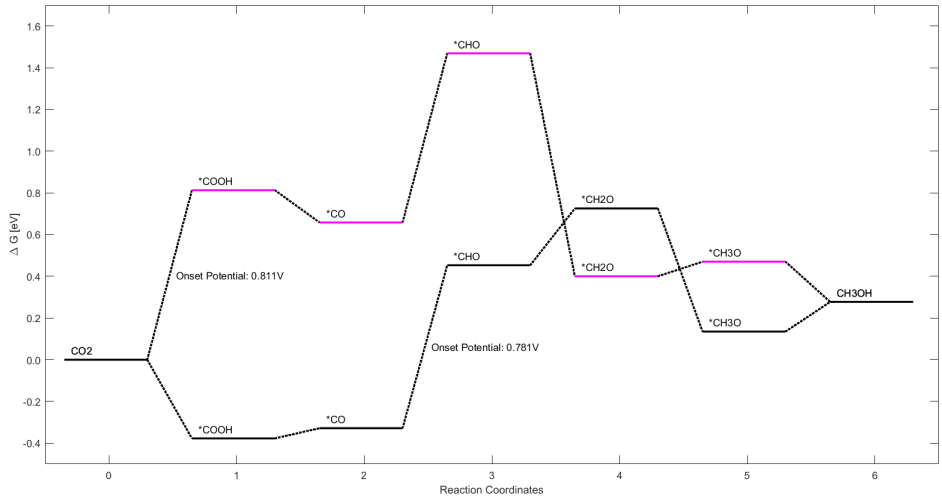

Figure 13: The figure shows the free energy diagram of the best CH_3OH producing pathway on the Cu78-type1 NP along with the same pathway on a (111) Cu layer

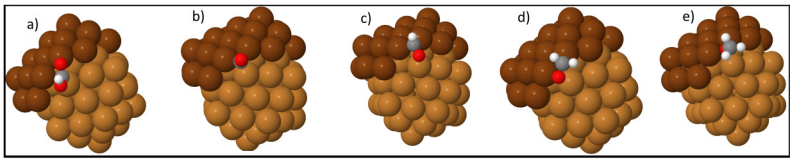

Figure 14: The figure shows the adsorbtion sites of the best pathway for CH_3OH production with the chemicals being: a)$COOH$, b)C, c)CHO, d)CH_2O, e)CH_3O

Adsorbate	Optimized structure	E_b	Adsorbate	Optimized structure	E_b
$^*COOH$	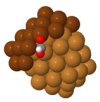	0.810	$^*CO$	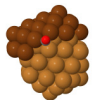	0.589
$^*CHO$		1.090	$^*COH$	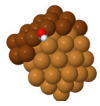	1.764
$^*CHOH$		1.486	$^*CH_2O$	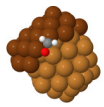	0.713
$^*CH_2OH$		0.666	$^*CH_3O$	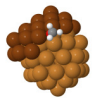	-0.447
$^*CH_3$		-0.368	$^*CH_2$		0.671
$^*H_2O$		-0.262	$^*H$		-0.188
$^*O$	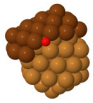	0.176	$^*OH$	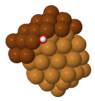	-0.499
$^*C$		2.124	$^*CH$	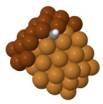	1.187

Table 2: Table of the adsorbate groups, their adsorbation sites and their bonding energy on a Cu78-type1 NP.

3.3 Cu78-type2 NP

3.3.1 Free energy Diagram

The best adsorbtion sites were found to be on the top and bottom of the Cu78-type2 NP. The adsorbtion was similar to the previous Cu78-type1 NP, with the intermediates before and with *CH_2O adsorbing slightly worse on the Cu78-type 2 NP, but the intermediates after *CH_2O adsorbing better. The onset potential of the LEP is between the Cu55 and the Cu78-type1. This pathway has the same PLS as the Cu55 NP.

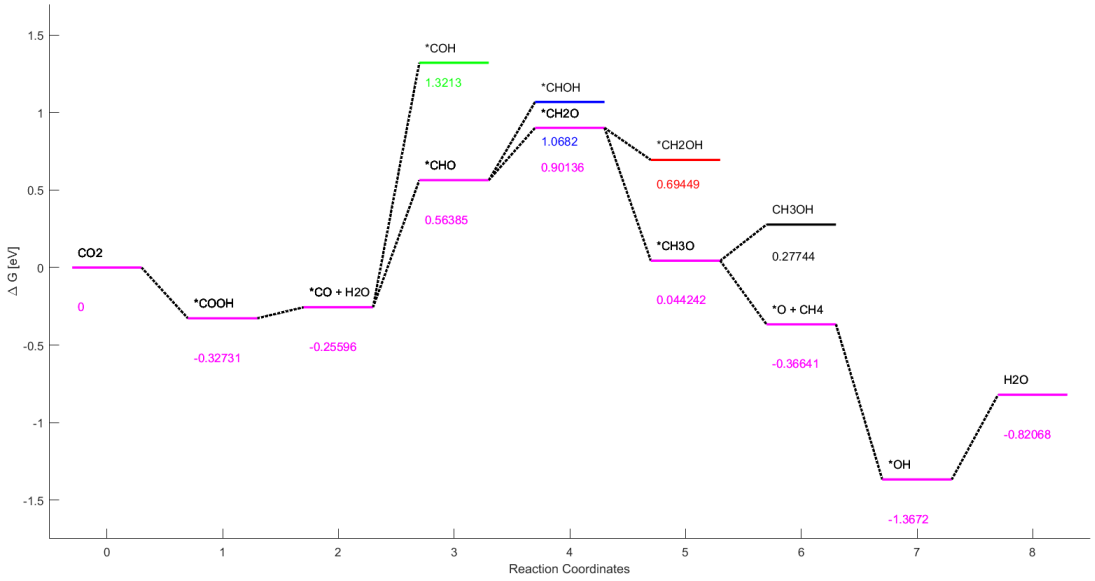

Figure 15: The figure shows FED of the Cu78-type2 NP with both methane and methanol pathways alongside other pathways.

3.3.2 CH_4 Production

Best pathway for CH_4 production on the Cu78-type2 NP was identified as

$$CO_2 \rightarrow^* COOH \rightarrow^* CO \rightarrow^* CHO \rightarrow^* CH_2O \rightarrow^* CH_3O \rightarrow^* O \rightarrow^* OH \rightarrow H2O \tag{8}$$

where * denotes that the chemical compound is adsorbed onto the Cu78-type2 NP.

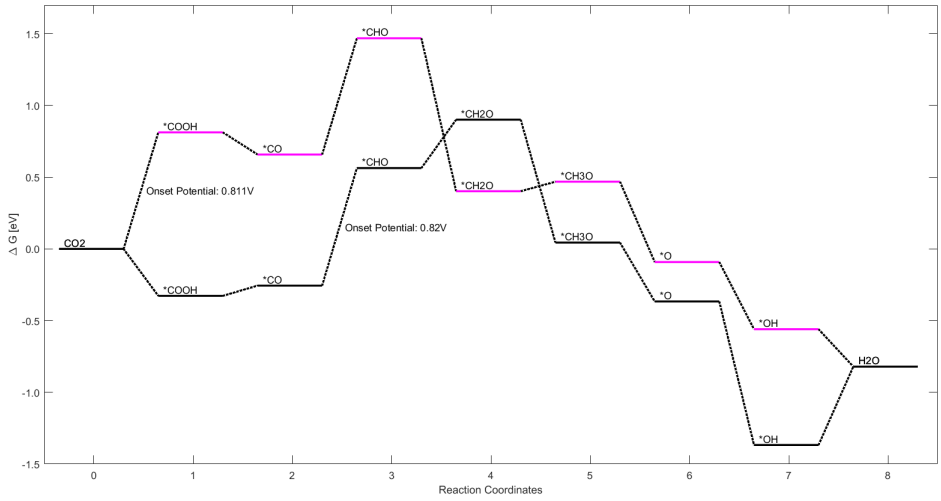

Figure 16: The figure shows the free energy diagram of the best CH_4 producing pathway on the Cu78-type2 NP along with the same pathway on a (111) Cu layer

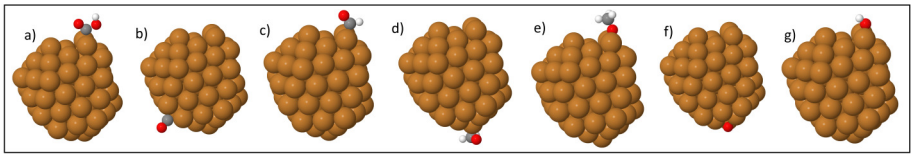

Figure 17: The figure shows the adsorbtion sites of the best pathway for CH_4 with the chemicals being: a)$COOH$, b)CO, c)CHO, d)CH_2O, e)CH_3O, f)O, g)OH

3.3.3 CH_3OH Production

Best pathway for CH_3OH production was identified as

$$CO_2 \rightarrow^* COOH \rightarrow^* CO \rightarrow^* CHO \rightarrow^* CH_2O \rightarrow^* CH_3O \rightarrow^* CH_3OH \tag{9}$$

where * denotes that the chemical compound is adsorbed onto the NP.

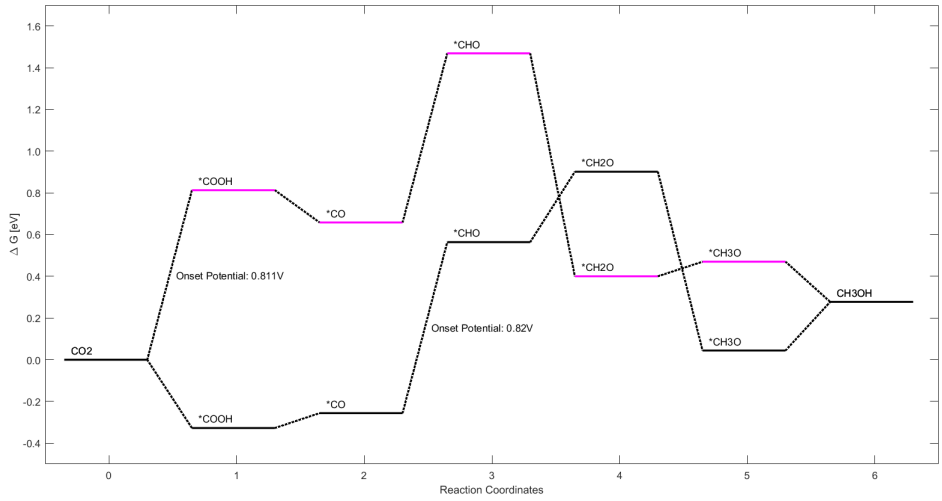

Figure 18: The figure shows the free energy diagram of the best CH_3OH producing pathway on the Cu78-type2 NP along with the same pathway on a (111) Cu layer

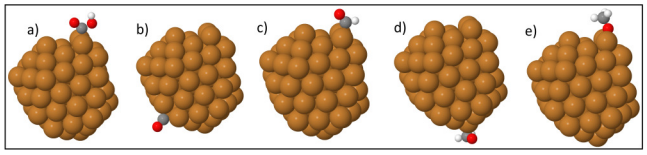

Figure 19: The figure shows the adsorbtion sites of the best pathway for CH_3OH production with the chemicals being: a)$COOH$, b)CO, c)CHO, d)CH_2O, e)CH_3O

Adsorbate	Optimized structure	E_b	Adsorbate	Optimized structure	E_b
$^*COOH$		0.860	$^*CO$		0.662
$^*CHO$		1.201	$^*COH$		2.149
$^*CHOH$		1.336	$^*CH_2O$		0.889
$^*CH_2OH$		0.652	$^*CH_3O$		-0.538
$^*CH_3$		-0.504	$^*CH_2$		0.651
$^*H_2O$		-0.336	$^*H$		-0.191
$^*O$		0.414	$^*OH$		-0.657
$^*C$		1.939	$^*CH$		0.964

Table 3: Table of the adsorbate groups, their adsorbation sites and their bonding energy on a Cu78-type2 NP.

3.4 Cu147 NP

3.4.1 Free energy Diagram

The best adsorbtion sites were found to be on and around the corners of the Cu147 NP. The adsorptions of the intermediates on the Cu147 NP is very similar to the adsorption of the Cu78-type1, with it in general being a bit worse at adsorbing than the Cu78-type1 NP. The Onset potential turned out to be slightly larger than that of the Cu55 NP. This pathway has the same PLS as the Cu55 NP.

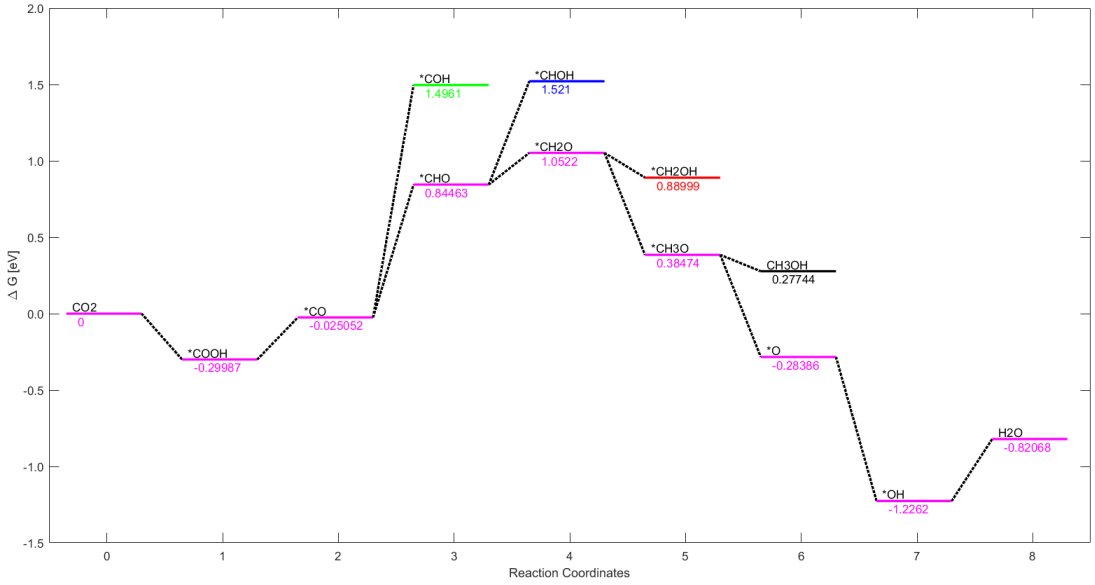

Figure 20: The figure shows FED of the Cu147 NP with both methane and methanol pathways alongside other pathways.

3.4.2 CH_4 Production

Best pathway for CH_4 production on the Cu147 NP was identified as

$$CO_2 \rightarrow^* COOH \rightarrow^* CO \rightarrow^* CHO \rightarrow^* CH_2O \rightarrow^* CH_3O \rightarrow^* O \rightarrow^* OH \rightarrow H2O \tag{10}$$

where * denotes that the chemical compound is adsorbed onto the Cu147 NP.

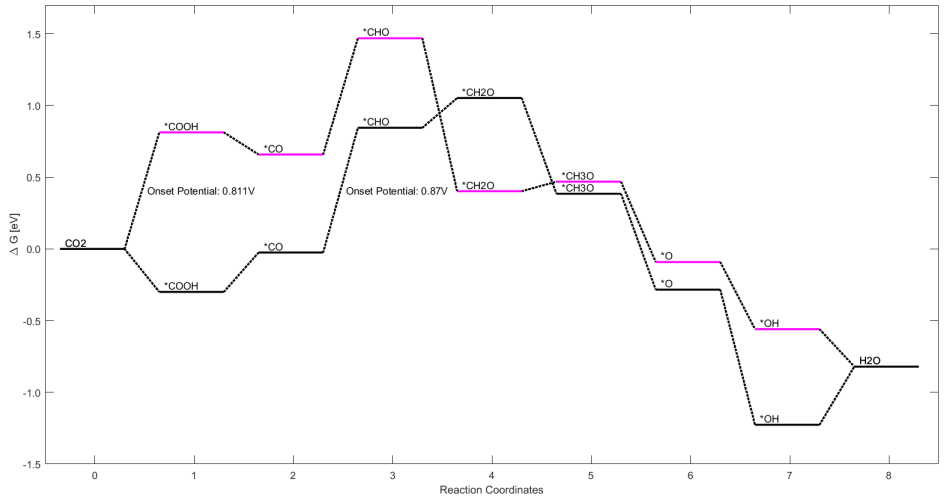

Figure 21: The figure shows the free energy diagram of the best CH_4 producing pathway on the Cu147 NP along with the same pathway on a (111) Cu layer

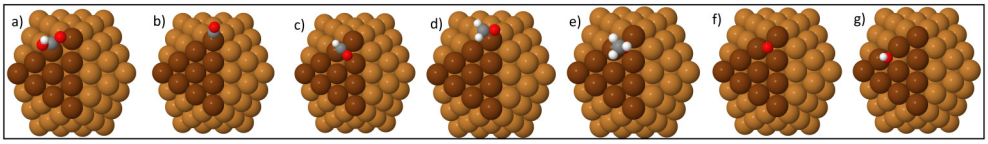

Figure 22: The figure shows the adsorbtion sites of the best pathway for CH_4 with the chemicals being: a)$COOH$, b)CO, c)CHO, d)CH_2O, e)CH_3O, f)O, g)OH

3.4.3 CH_3OH Production

Best pathway for CH_3OH production was identified as

$$CO_2 \rightarrow^* COOH \rightarrow^* CO \rightarrow^* CHO \rightarrow^* CH_2O \rightarrow^* CH_3O \rightarrow^* CH_3OH \tag{11}$$

where * denotes that the chemical compound is adsorbed onto the Cu147 NP.

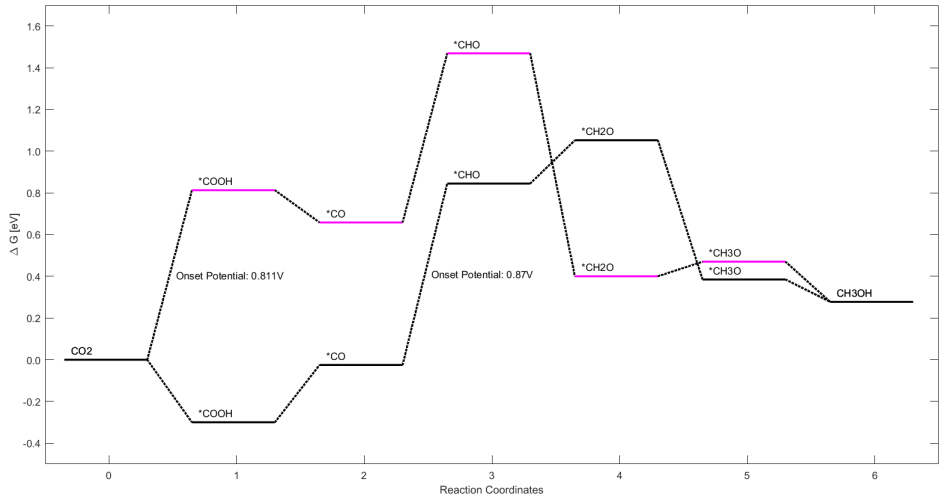

Figure 23: The figure shows the free energy diagram of the best CH_3OH producing pathway on the Cu147 NP along with the same pathway on a (111) Cu layer

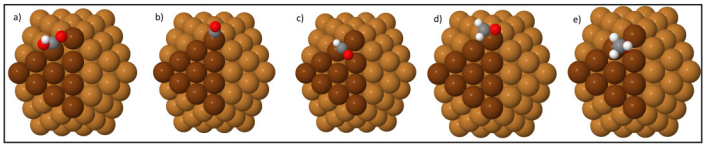

Figure 24: The figure shows the adsorbtion sites of the best pathway for CH_3OH production with the chemicals being: a)$COOH$, b)CO, c)CHO, d)CH_2O, e)CH_3O

Adsorbate	Optimized structure	E_b	Adsorbate	Optimized structure	E_b
$^*COOH$		0.888	$^*CO$		0.892
$^*CHO$		1.482	$^*COH$		2.324
$^*CHOH$		1.789	$^*CH_2O$		1.040
$^*CH_2OH$		0.848	$^*CH_3O$		-0.198
$^*CH_3$		-0.170	$^*CH_2$		0.956
$^*H_2O$		-0.242	$^*H$		-0.005
$^*O$		0.497	$^*OH$		-0.195
$^*C$		2.807	$^*CH$		1.706

Table 4: Table of the adsorbate groups, their adsorbation sites and their bonding energy on a Cu147 NP.

3.5 Comparison diagrams

3.5.1 Comparison pathway of CH_4 Production

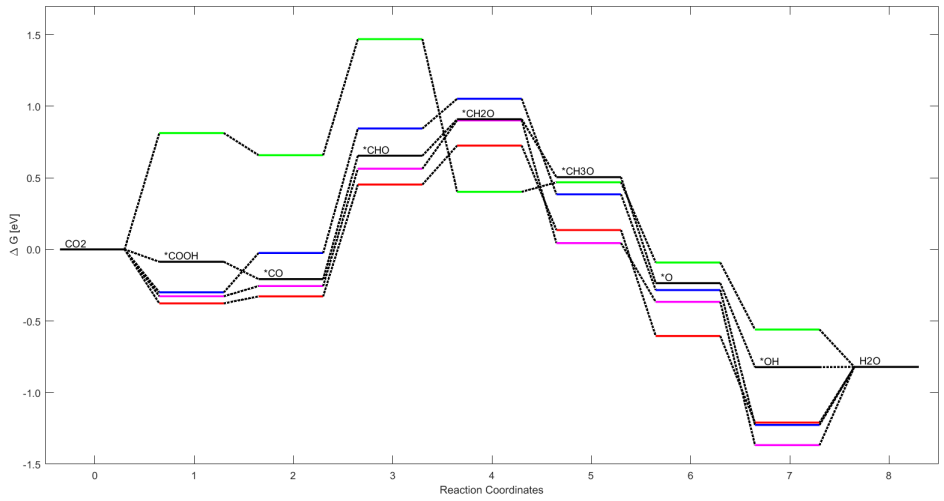

Figure 25: Figure shows the CH_4 producing pathway on the 4 different Cu NP/surfaces, with Green being the (111) surface, black being Cu55, red being Cu78-type1, pink being Cu78-type2 and blue being Cu147.

3.5.2 Comparison pathway of CH_3OH Production

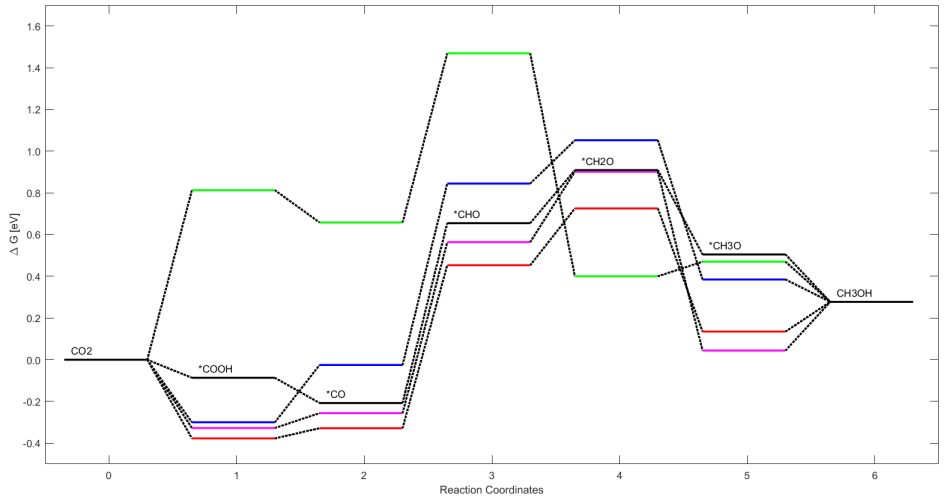

Figure 26: Figure shows the CH_3OH producing pathway on the 4 different Cu NP/surfaces, with Green being the (111) surface, black being Cu55, red being Cu78-type1, pink being Cu78-type2 and blue being Cu147.

3.6 Comparison between NP's, flat surface and A/B/533 Cu structures

The following sections feature the LEPs of the NPs alongside the LEPs of a flat Cu(111) surface and the jagged edge strucures A01, A13, A33, B11 -, B33, B55, B221, 553-system1 and 553-system2.

3.6.1 Bargraph of the onset potential of different structures

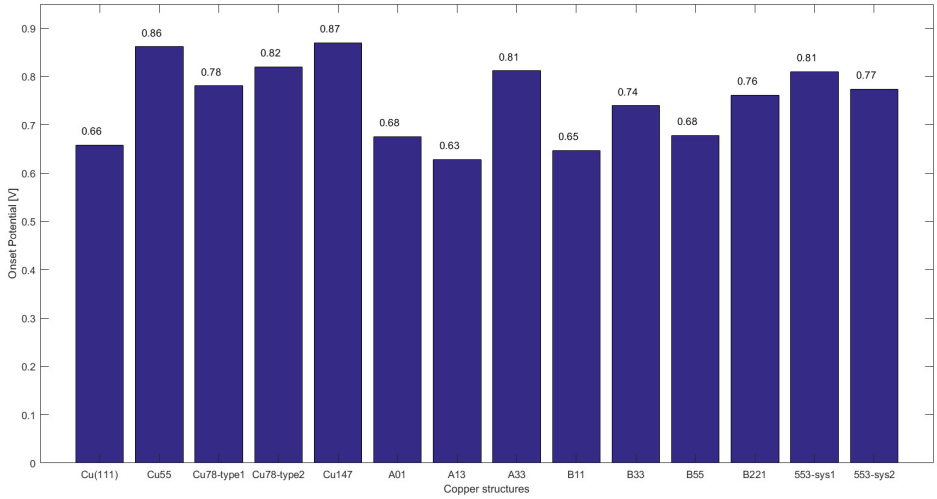

Figure 27: Figure shows the onset potentials of the LEP of various different Cu structures.

3.6.2 Best LEP of the 3 categories

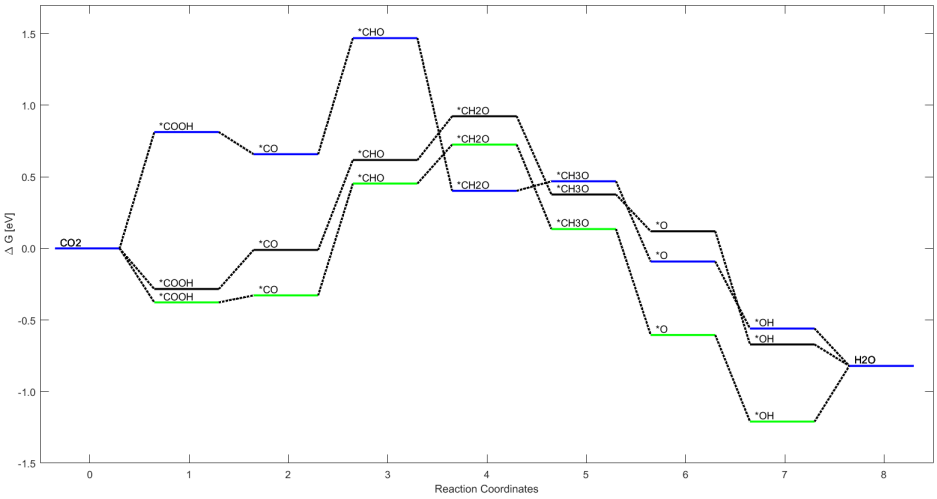

Figure 28: Figure shows the LEP of the lowest onset potential structure in each category, with Cu(111) in blue, Cu78-type1 in green and A13 in black

3.6.3 Lowest energy methane and methanol producing pathways of the A/B/553 structures

The following graphs show the LEP that result in the production of methane and methanol for the A, B and 553 structures.

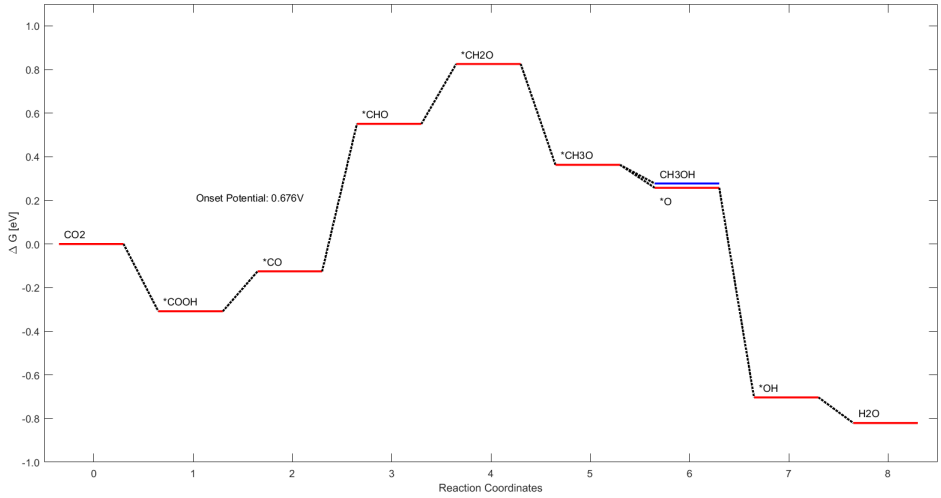

Figure 29: The figure shows the LEP of methanol and methane production for the A01 structure

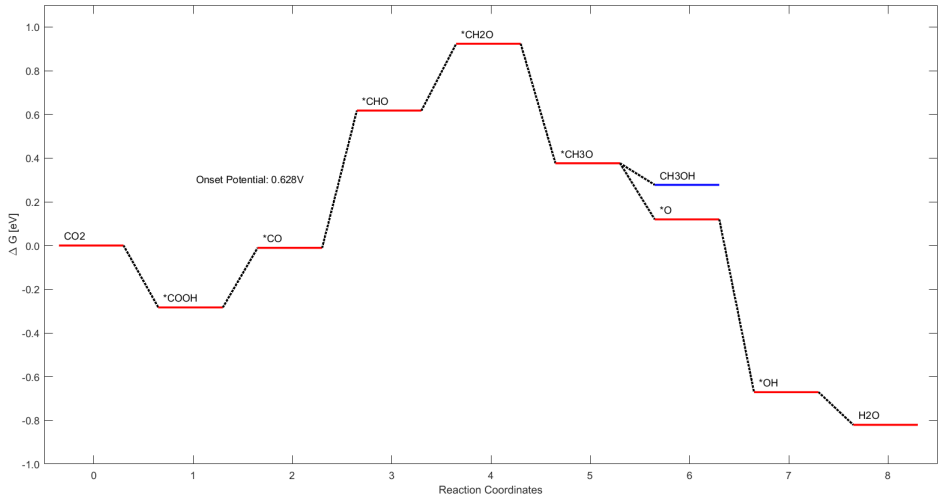

Figure 30: The figure shows the LEP of methanol and methane production for the A13 structure

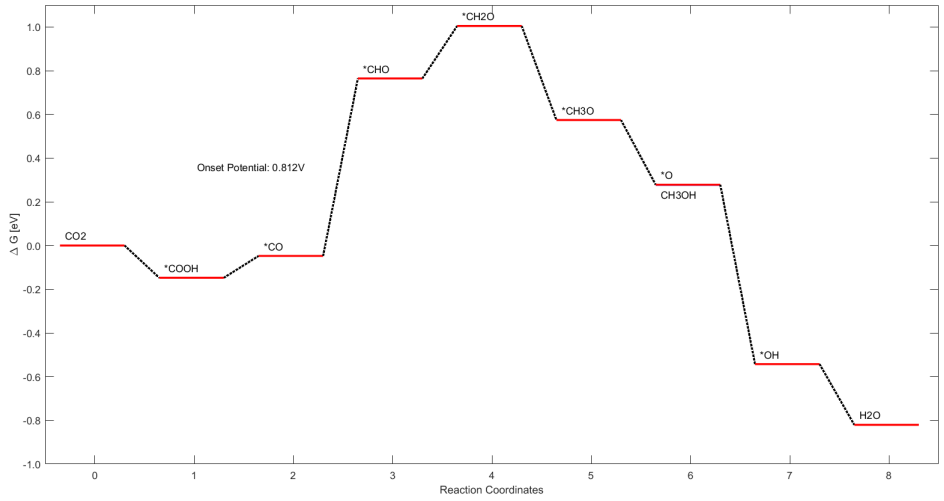

Figure 31: The figure shows the LEP of methanol and methane production for the A33 structure

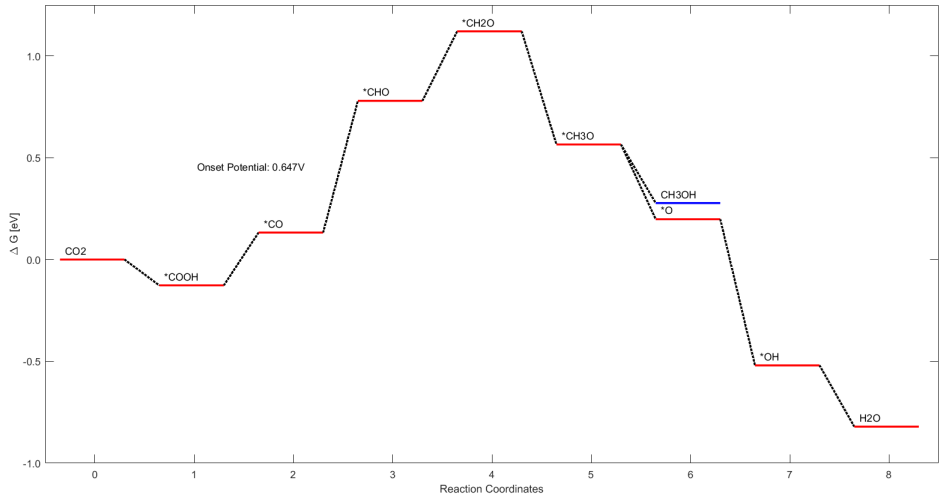

Figure 32: The figure shows the LEP of methanol and methane production for the B11 structure

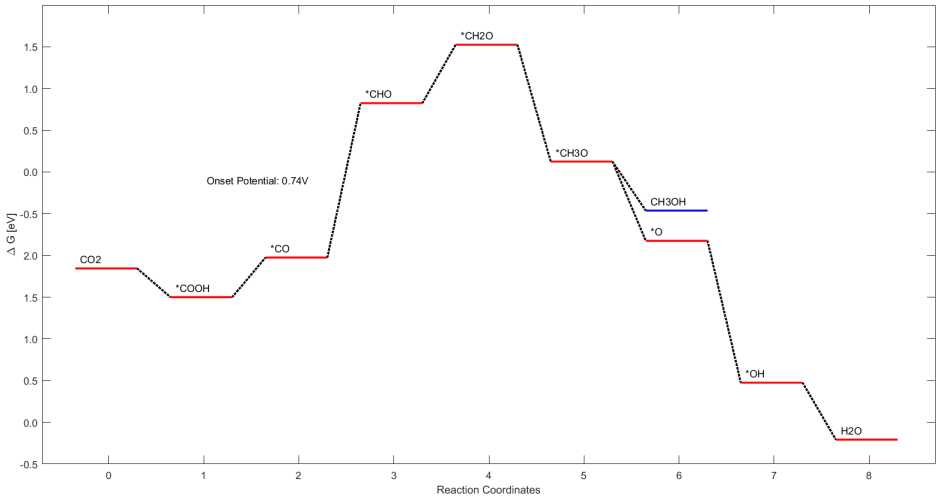

Figure 33: The figure shows the LEP of methanol and methane production for the B33 structure

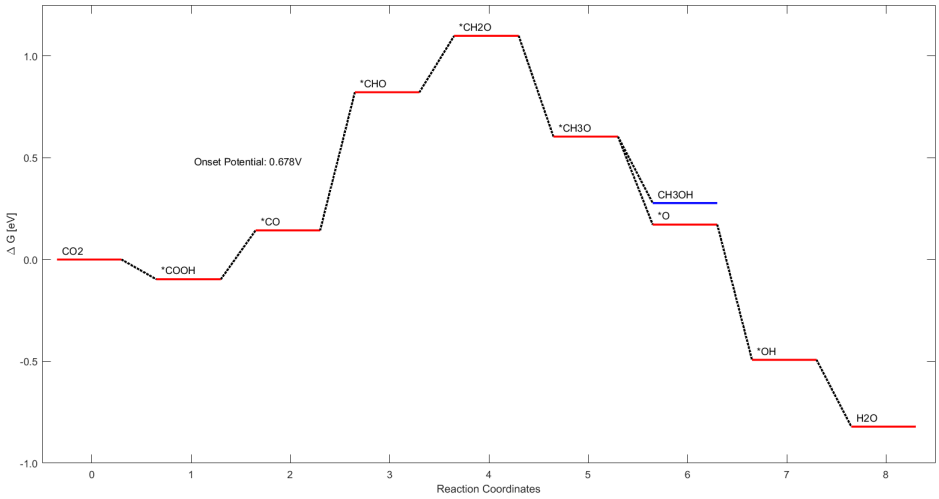

Figure 34: The figure shows the LEP of methanol and methane production for the B55 structure

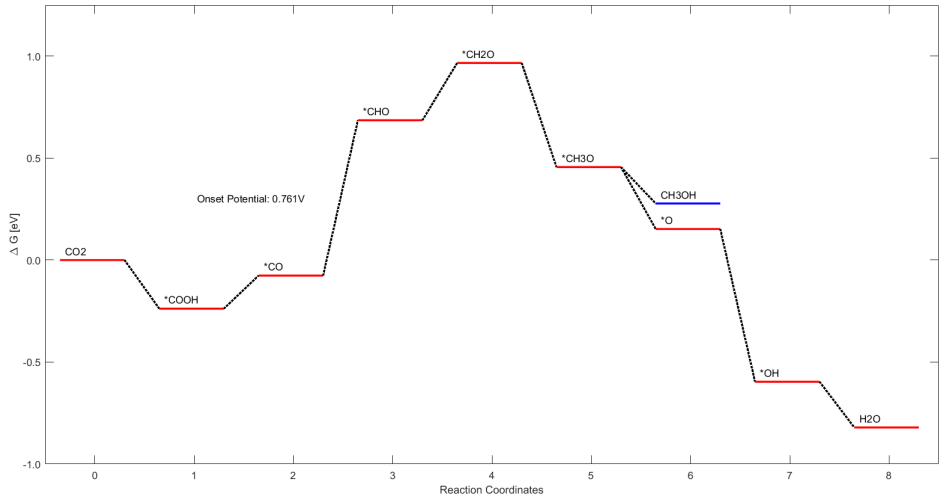

Figure 35: The figure shows the LEP of methanol and methane production for the B221 structure

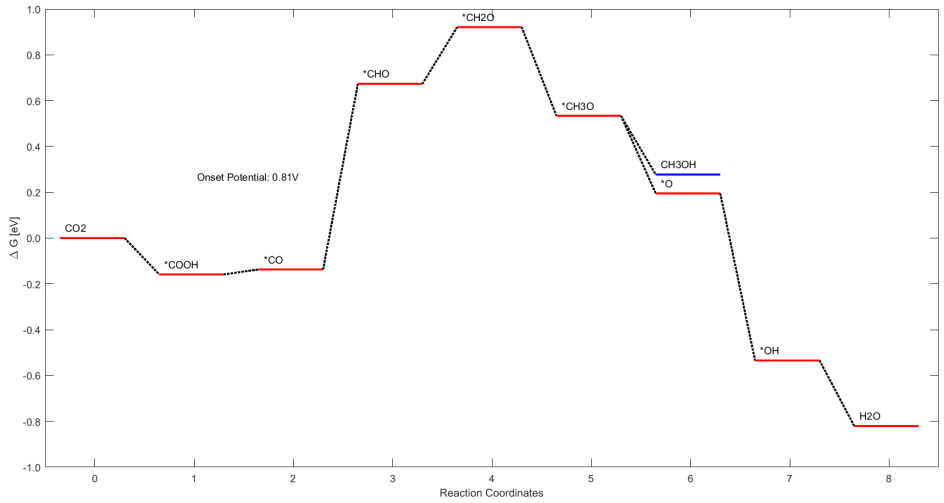

Figure 36: The figure shows the LEP of methanol and methane production for the 553-system1 structure

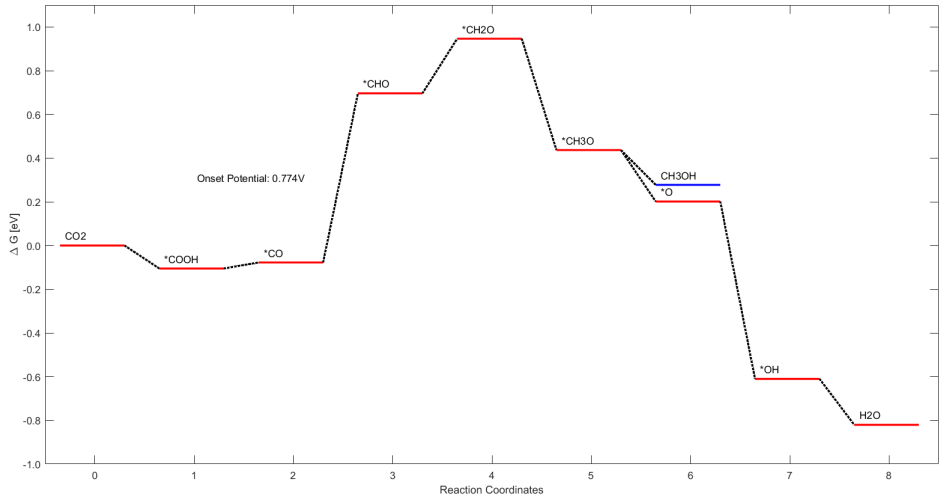

Figure 37: The figure shows the LEP of methanol and methane production for the 553-system2 structure

4 Conclusion

From this investigation, we conclude that the Cu NPs all have the same reaction pathway for both methane and methanol formation. The free energy landscape is similar for all the NPs but it is qualitatively very different from the Cu(111) surface. The NPs have one distinct potential limiting step, the $*CO$ to $*CHO$ step, while two reaction steps are potential limiting for the Cu(111) surface, the CO_2 to $*COOH$ and the $*CO$ to $*CHO$ step. Only the Cu78-type1 NP proved to have an onset potential slightly lower than that of Cu(111), but the onset potentials are very similar for all the NPs and the Cu(111) surface. The adsorbed species are shown to be more stable on the Cu NPs with the exception of $*CH_2O$ being more stable on the Cu(111) surface (and $*CH_3O$ in one case). For the more crucial steps, the Cu NPs proved to adsorb the intermediates considerably more than the Cu(111) surface, where reduction of CO_2 to $*CO$ is much more facile on the NPs than on the Cu(111) surface.